CMS Draft Analysis Note

2010/11/22
Head Id: 1.0
Archive Id:
Archive Date:

Search for Collimated Groups of Muons

Jim Pivarski, Alexei Safonov, Aysen Tatarinov

Abstract

We present an inclusive, signature-based search for groups of collimated muons with the CMS detector. Groups of collimated muons may originate in high-momentum cascades from LHC pp collisions into as-yet unknown low-mass states of a hidden-valley sector of new physics. In several well-defined acceptance regions (single $p_T > 80$ GeV/c dimuon, single collimated quadmuon, two collimated dimuons, one dimuon and one quadmuon, and two quadmuons), trigger and reconstruction efficiencies are independent of the kinematics of the decay and backgrounds are at the level of 1 pb and lower, estimated using data-driven techniques. A mass-peak fit is used to set limits/discover new resonances with XX sensitivity in 35 pb^{-1}. We use these results to set limits on several representative benchmark models (almost, must w/ dark sector)

This box is only visible in draft mode. Please make sure the values below make sense.

PDFAuthor:	CMS Collaboration
PDFTitle:	Search for Collimated Groups of Muons
PDFSubject:	CMS
PDFKeywords:	CMS, physics, exotica, muons

Please also verify that the abstract does not use any user defined symbols

1 Introduction

FIXME: Needs a lot of references.

Although the dimuon mass spectrum is well understood in e^+e^- and $p\bar{p}$ collisions up to 0.2 and 2 TeV respectively, (**FIXME:** get real numbers) new states may be hidden by weak couplings. A wide class of hidden-valley models predicts new states coupling weakly to the Standard Model yet significantly to a hidden sector, with strong mixing between the Standard Model and the hidden sector only at high collision energies. In such scenarios, heavy particles M can only be produced with significant cross-section at the LHC, but they can then decay through the whole spectrum to the lightest hidden state: $pp \to M\overline{M}$ and $M \to mX$ where m is a low-mass state. The lightest hidden state is either stable (which makes the whole chain invisible) or decays with very small width to the accessible Standard Model states, either democratically (Z-like) or to the heaviest accessible state (Higgs-like). If one of these final states is a muon pair, it would appear in CMS as a low-mass, high-momentum dimuon. If there are several low-mass states in the decay chain, e.g. m_1 and m_2, then $m_2 \to m_1 m_1 \to 4\mu$ cascades would either produce two groups of collimated dimuons or one group of four collimated muons (a "quadmuon"), depending on the boost of m_2. Arbitrarily complex decay chains are conceivable, and groups of muons might be produced in association with other Standard Model pairs, such as e^+e^- and $\pi\pi$. These striking signatures are often called "lepton jets."

Hidden, low-mass resonances are especially interesting in light of the high-energy positron excess recently discovered by the PAMELA primary cosmic-ray experiment. This excess of interstellar positrons could be the product of WIMP annihilations, assuming that the WIMP annihilation rate is higher than what would be expected from thermal freeze-out in the early universe, and also assuming some mechanism to prohibit decay chains that produce antiprotons, in which no excess was observed. A new force boson, z_{dark}, with a mass of approximately 1 GeV/c^2 and coupling significantly to WIMPs yet weakly to Standard Model particles, would explain both observations. Acting as a long-range Yukawa force, z_{dark} would draw together slow-moving WIMPs, increasing their effective cross-section in the modern era without affecting their production in the early universe. As a decay channel, $z_{\text{dark}} \to X \to p\bar{p}$ would be kinematically forbidden if the mass of z_{dark} were above 2 GeV/c^2 or so. Relatively simple extensions of this picture, such as adding a dark Higgs boson h_{dark} to give the z_{dark} a mass, or introducing the force as a non-abelian group, would produce more complex event topologies: 2^N fermion pairs per lepton jet for an N-state decay chain and/or several lepton jets per event.

Another, very different, motivation derives from the tension between the low Higgs mass predicted by precision electroweak fits and the direct LEP limit of 114 GeV/c^2. This limit assumes that the Higgs boson decays directly into Standard Model particles with known branching fractions. If multiple Higgs bosons allow for Higgs-to-Higgs

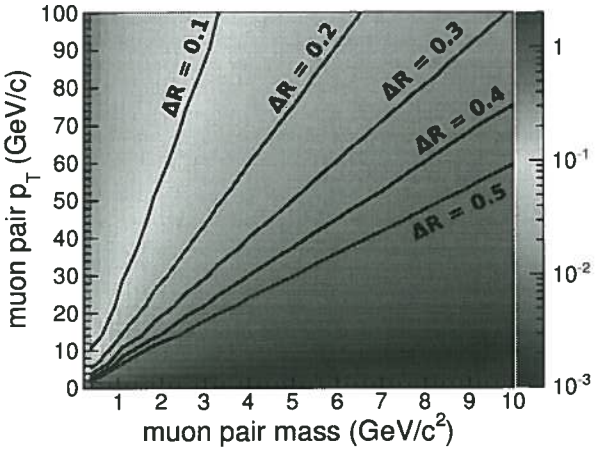

Figure 1: Relationship between ΔR (represented by color scale and contour lines) and the mass and momentum of a pair of muons (isotropically generated, decay as scalars). Lines of constant boost (energy divided by mass) have roughly constant ΔR.

decays, the direct limit may be circumvented. In a well-defined region of Next-to Minimal SuperSymmetric (NMSSM) parameter space, the lightest CP-odd Higgs (a_1) can have arbitrarily low mass. Below the $2m_\tau$ threshold, the branching fraction for $a_1 \to \mu\mu$ is about 20%. For values of the NMSSM parameters that give the lightest CP-even Higgs (h_1) a large singlet field component, $h_1 \to a_1 a_1$ can be as large as 100%. If nature has chosen this model, then the Higgs mass could be as low as 86 GeV/c^2 and the primary Higgs signature would be $h_1 \to a_1 a_1 \to 2\mu, 2\mu$, where the dimuons appear as two well-collimated lepton jets.

In this paper, we present an inclusive, signature-based search for collimated groups of muons with arbitrarily many muons in each group ("mu-jets"). No additional objects, such as hadronic jets or missing energy, are required in the search, though they are not forbidden, either. To avoid eliminating lepton jets with e^+e^- or $\pi\pi$ in addition to the muons, isolation is not required in the signal channels.

Because the generic phenomenon of interest is a new spectrum of neutral resonances with well-defined masses, we iteratively group oppositely-signed pairs of muons into mu-jets if the pairs have small invariant masses (less than 5 GeV/c^2), rather than small geometric angles $\Delta R = \sqrt{(\Delta\phi)^2 + (\Delta\eta)^2}$. We therefore identify cascades within a rectangular region of the plane of theoretically possible masses and momenta, rather than a triangular one (see Fig. 1). This mu-jet clustering algorithm could be seen as a logical extension of the "shrinking cone" used to reconstruct hadronic taus, which is also designed to select a fixed-mass resonance over a wide range of momenta. In the case of mu-jets, however, the mass of the final-state muons can be fully reconstructed, so the "shrinking" of ΔR with high momentum can be more easily achieved by simply

selecting pairs by mass.

We assume that all cascade chains end in a single lightest hidden state, m_1, before decaying into muons, which is to say that the coupling of hidden states to each other is much greater than the coupling of any of them to the Standard Model. Thus, an event may have many m_1 particles decaying into dimuons, but all of these dimuons have the same mass, which greatly simplifies the search. Some of these dimuons may be overlapping each other in the same mu-jet, so in mu-jets containing four or more muons, we identify the combination of oppositely-signed dimuons that are most consistent with a single m_1 mass, and call them "fundamental dimuons."

Signal channels are classified by the number of mu-jets and the number of muons in each mu-jet, motivated by different signal topologies and background levels. These channels are:

(a) a single dimuon (~~two-muon~~ mu-jet) with $p_T > 80$ GeV/c (p_T is the vector sum of all muons in the mu-jet), targeting models with a single energetic $m_1 \to \mu\mu$ (**FIXME:** this 80 GeV/c threshold hasn't been optimized);

(b) a single quadmuon (four-muon mu-jet), targeting models with one low-mass m_2 decaying via $m_2 \to m_1 m_1 \to 4\mu$;

(c) a single mu-jet with more than four muons, targeting more complex cascades;

(d) two mu-jets in the following cases:

- (d-1) each mu-jet contains two muons, targeting a model with a heavy particle decaying to two light particles: $M \to m_1 m_1 \to 4\mu$ (this is the NMSSM signature),
- (d-2) one mu-jet contains two muons, the other four: $M \to m_1 m_2$, with $m_1 \to \mu\mu$ and $m_2 \to m_1 m_1 \to 4\mu$,
- (d-3) both contain four: $M \to m_2 m_2$,
- (d-4) either mu-jet contains more than four (complex cascades);

(e) more than two mu-jets (complex cascades).

Any additional, un-grouped muons are ignored. Within the grouped muons, the following channels have a well-defined number of fundamental dimuons per event: (a) has one, (b) and (d-1) have two, (d-2) has three, where one pair of fundamental dimuons is identified within a mu-jet, and (d-3) has four fundamental dimuons, all identified within mu-jets. The "overflow bins," (c), (d-4), and (e), can have arbitrarily many fundamental dimuons.

In each channel, we search for an excess above background using a fit to fundamental dimuon mass and interpret such an excess as the lightest hidden resonance m_1.

In a channel with N fundamental dimuons, the fit function is N-dimensional with N measured dimuon masses per event. The mass of the lightest hidden state is a single parameter, so the signal is constrained to a diagonal in the N-dimensional space, with the entire off-diagonal region providing mass-sidebands to determine background levels from data. The shape of the background fit function is taken as a template from a background-only control sample. If an m_1 mass peak is discovered in an N-dimuon fit, then the four-muon masses will be added as another parameter in the fit to search for $m_2 \to m_1 m_1 \to 4\mu$, and so on, up the observed chain.

To avoid model bias introduced by the shapes of the trigger turn-on curves or detector efficiency as a function of muon p_T and η, we define acceptance regions within which the trigger and reconstruction efficiencies are constant. This is to provide a result that can be directly applied to new theoretical models without detailed multi-dimensional descriptions of the detector efficiency. The efficiency curves that are avoided depend on the degree of overlap of the muon trajectories through CMS, which has a complicated shape as a function of muon mass and momentum (or equivalently, ΔR and momentum). In brief, these acceptance cuts are

- at least one muon with $p_T > 15$ GeV/c and $|\eta| < 1$ per event;
- all other muons must have $p_T > 5$ GeV/c and $|\eta| < 2.4$.

To the extent that the new resonances are highly boosted, this is equivalent to the following:

- at least one mu-jet with $p_T > 20$ GeV/c and $|\eta| < 1$ per event;
- all other mu-jets (if any) with $p_T > 10$ GeV/c and $|\eta| < 2.4$.

for mass < 5 GeV/c^2 mu-jets.

A single trigger efficiency correction and one offline efficiency correction (raised to the number of muons per channel) is applied to the final result: these corrections are derived from $J/\psi \to \mu\mu$ tag-and-probe with the same acceptance cuts.

FIXME: From this point onward, I freely use CMS jargon, only appropriate for the internal note.

2 Region of constant trigger efficiency

For all signal channels, we select events with the highest unprescaled, unisolated, single-muon trigger available. In the 2010A dataset (May–Aug 2010, 3 pb^{-1}), this is HLT_Mu9 and in the 2010B dataset (Sep–Oct 2010, 32 pb^{-1}), this is HLT_Mu11. (The HLT_Mu11 trigger is not available in the 2010A dataset, so they cannot be treated equally.) We additionally apply stricter offline cuts to be insensitive to the shape of the trigger turn-on curves.

CMS muon triggers are efficient for nearby muons within certain boundaries that motivate our choice of the unisolated, single-muon trigger and the offline acceptance cuts to guarantee uniform efficiency after cuts. The boundaries are:

- p_T (the threshold curves) and $|\eta|$ (extent of the detector), well-documented elsewhere (**FIXME:** reference?);
- double-muon triggers (e.g. HLT_DoubleMu3) are inefficient when the muons cross in the muon system (moderate boost, depends on kinematics);
- track-based isolation (e.g. in HLT_IsoMu9) excludes muons that are too close to one another in the pixel detector (very high boost only);
- the L1 endcap trigger is inefficient when the muons cross in the muon system. (**FIXME:** Only known to be due to L1 by process of elimination and one brief test, not a complete study that identifies the underlying cause.)

The last condition motivates the acceptance requirement of one high-momentum muon in the barrel ($|\eta| < 1$).

To investigate trigger and offline reconstruction efficiencies, a special Monte Carlo was generated with dimuons uniformly distributed in mass (a random mass was chosen in each event), pair p_T, and pair η. Instead of realistically modeling any physical process, this "dimuon gun" covers the space of possible dimuons ~~in a physically reasonable way~~, allowing us to search for inefficient regions. All trigger efficiencies quoted below are efficiencies for L1 and HLT combined, labeled by HLT path name.

The HLT_DoubleMu3 trigger has a complex efficiency profile for dimuons, presented in Fig. 2 with offline StandAloneMuon reconstruction efficiency for comparison. The HLT_DoubleMu3 trigger requires two GlobalMuons to be reconstructed in the HLT, and thus implicitly requires two StandAloneMuons. The StandAloneMuon profile reproduces the inefficiency between barrel wheels of HLT_DoubleMu3, but not the inefficiency at high $|\eta|$. Both inefficiency patterns are only substantial for low-mass, high-momentum dimuons: muons that are nearly parallel and overlapping in the muon system.

The effect of isolation in HLT_IsoMu9 is shown in Fig. 3 by comparison with HLT_Mu9. Both exhibit the same inefficiency at high $|\eta|$, but HLT_IsoMu9 additionally has an inefficiency for $p_T \gtrsim 50$ GeV/c dimuons at $|\eta| < 0.5$. The isolation is implemented by requiring an absence of pixel-tracks near the triggered muon, which is violated in high-momentum dimuons.

Figure 4 shows HLT_IsoMu9, HLT_Mu9, and HLT_Mu11 versus η only, so that quantitative efficiencies can be read from the plot. The unisolated, single-muon triggers have 95–100% efficiency in the barrel region ($|\eta| < 1$) but the efficiency curves to zero in the endcap, independent of p_T.

This inefficiency is strongest for muons that cross each other in the muon endcap. This

Unclear. I think you are saying that these triggers are not very efficient. It is very vague. You can be more clear!

Appendix?

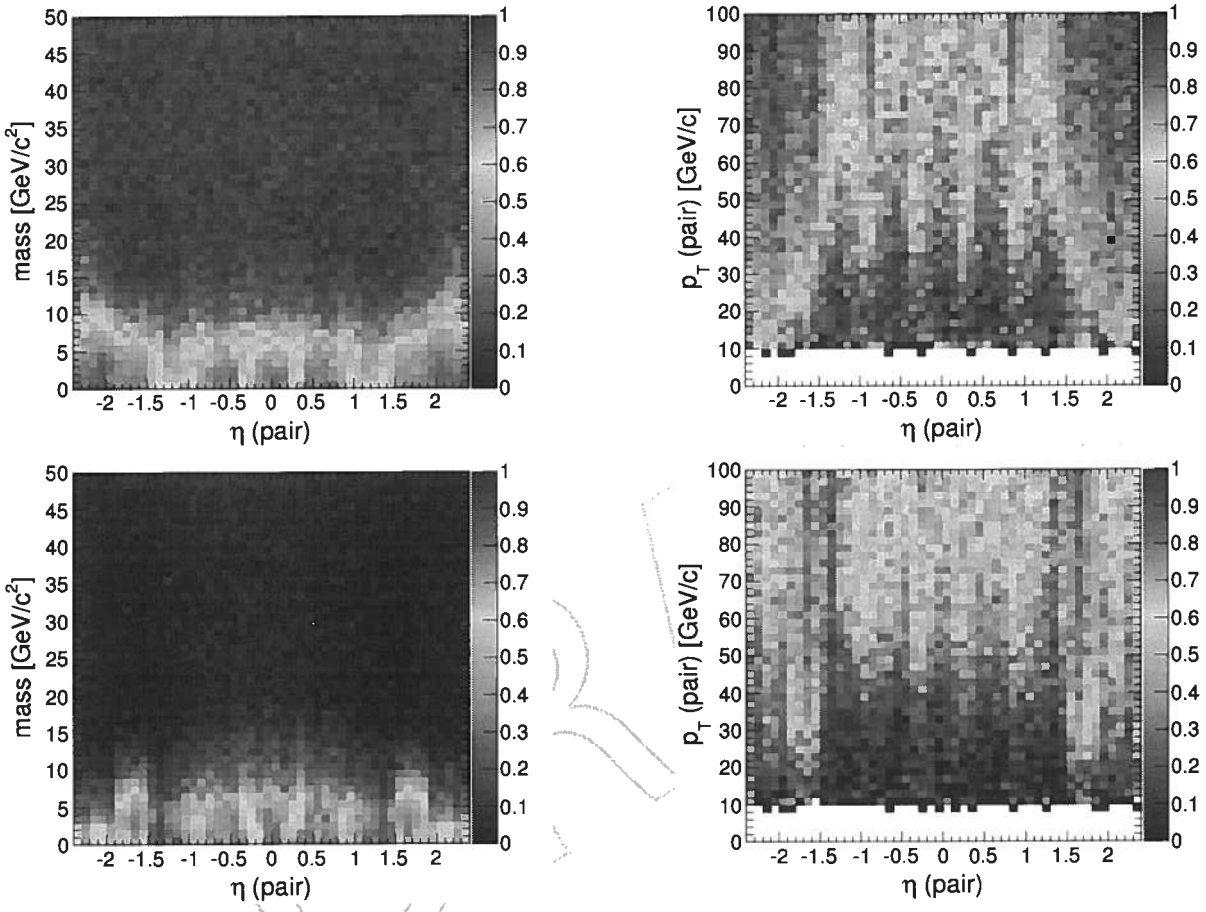

Figure 2: Top two plots: efficiency (color scale) of HLT_DoubleMu3 trigger as a function of dimuon mass, η, and p_T. Bottom two plots: probability to reconstruct two StandAloneMuons, a prerequisite for the HLT_DoubleMu3 trigger. Plots on the right are for mass $< 5\,\mathrm{GeV}/c^2$ only.

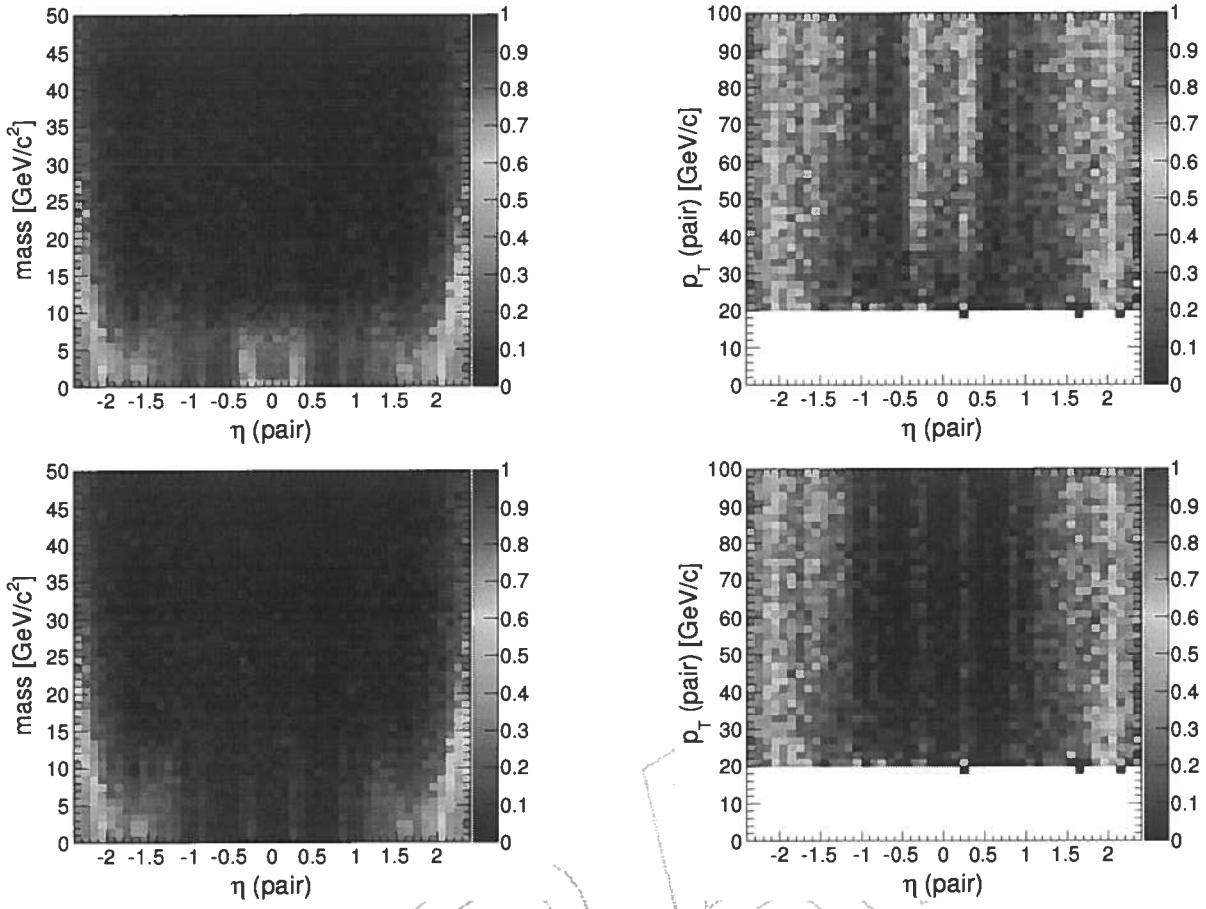

Figure 3: Top two plots: efficiency (color scale) of HLT_IsoMu9 trigger as a function of dimuon mass, η, and p_T. Bottom two plots: efficiency of HLT_Mu9, the same trigger without isolation. The denominator for all efficiencies includes at least one $p_T > 15$ GeV/c muon, and mass < 5 GeV/c^2 for plots on the right.

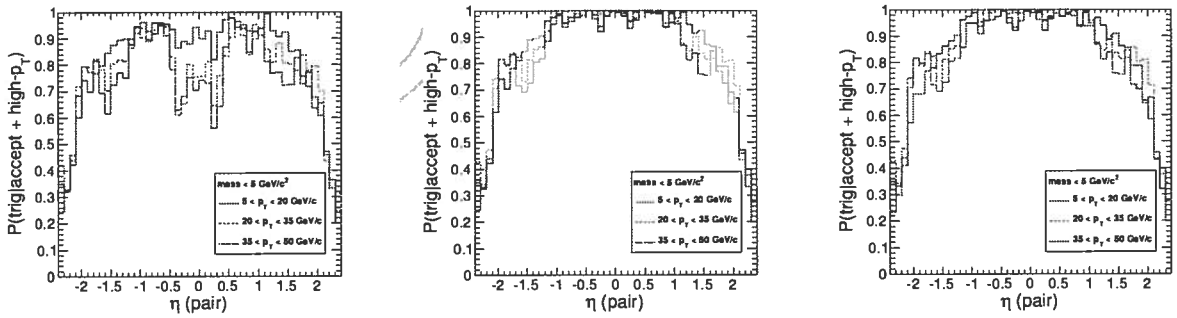

Figure 4: Trigger efficiency for HLT_IsoMu9 (left), HLT_Mu9 (middle), and HLT_Mu11 (right) for muon pairs in which both muons are in the specified p_T ranges. All muon pairs in this sample have invariant mass < 5 GeV/c^2 and at least one $p_T > 15$ GeV/c muon.

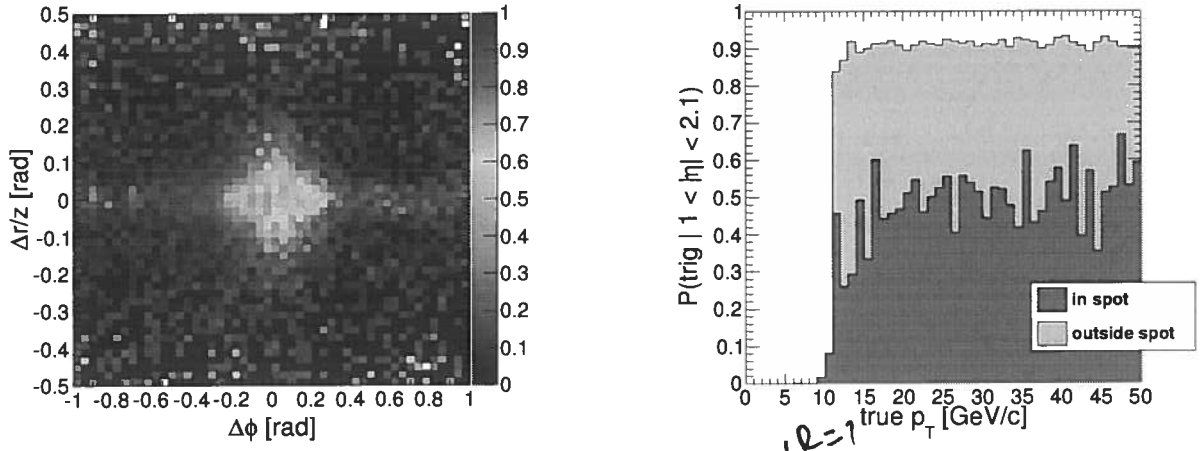

Figure 5: Left: endcap ($|\eta| < 1$) HLT_Mu11 efficiency as a function of where muon trajectories cross one another in the endcap (a plane at ± 700 cm). Right: HLT_Mu11 efficiency ($1 < |\eta| < 2.1$) as a function of the positive-muon p_T (the negative muon has $p_T < 9$ GeV/c to avoid satisfying the trigger). The "spot" is defined as $|\Delta\phi| < 0.2$ and $|\Delta r/z| < 0.1$.

can be seen by plotting the efficiency as a function of difference in muon trajectories evaluated in the detector, rather than the interaction point. Two planes, one at 700 cm and the other at -700 cm from the interaction point were used to represent the two endcaps, and generator-level muon trajectories were propagated through the CMS magnetic field to these planes, where their positions were compared in two dimensions: $\Delta\phi$ (difference in azimuthal angle) and $\Delta r/z$ (difference in radial position divided by 700 cm).

Figure 5 shows the HLT_Mu11 endcap efficiency as a function of crossing distance and p_T: the efficiency is localized to muons that nearly cross one another, but is independent of p_T. The probability to reconstruct one of the two muons as an offline StandAloneMuon or GlobalMuon is nearly 100% for all crossing distances, p_T, and η, implying that this inefficiency is in L1, rather than HLT. **FIXME:** I have one plot from Vadim by e-mail showing positively that this is an L1 issue (rather than just deducing it from process of elimination, as I do here, but it's a single plot versus ΔR. It would be good to put it in the same form as the rest of these, possibly investigating it with more variables ($\Delta\phi$, $\Delta r/z$, p_T, η).

If we did not explicitly require one offline high-p_T muon with $|\eta| < 1$, then different physics models would be sensitive to this inefficiency to different degrees, depending on how they populate the p_T, η plane and what masses they predict. It would be difficult to provide this information in a useful way, since it depends on several variables, some of which are obtained by propagating muon trajectories through the CMS magnetic field. We therefore require at least one offline muon with $p_T > 15$ GeV/c, $|\eta| < 1$ muon in every signal channel, thus guaranteeing that HLT_Mu9 and HLT_Mu11 are in

the plateau region of p_T and are insensitive to whether muons cross in the detector. Measurement of the trigger efficiency in the plateau region is covered in Sec. 4.

3 Offline muon reconstruction and identification

All offline muons in this analysis are selected to have the following properties:

- $p_T > 5$ GeV/c and $|\eta| < 2.4$;
- identified with the TrackerMuon algorithm (tracker-track matched to muon segments, the inside-out muon identification);
- at least two fully arbitrated (SegmentAndTrackArbitration) muon segments;
- number of hits in the tracker ≥ 8;
- track χ^2/N_{dof} in the tracker < 4.

3.1 Offline muon efficiency

The most unusual choice in the above is the use of TrackerMuons for high-momentum muons: this is motivated by the fact that the TrackerMuon (inside-out) algorithm is more robust than the GlobalMuon (outside-in) algorithm for identifying all muons when they cross one another in the muon system. The point of failure for the GlobalMuon algorithm is in the stage where a StandAloneMuon is built from segments. The TrackerMuon algorithm only requires segments, so it is insensitive to this effect.

To quantify this inefficiency, we again cover all possible dimuon kinematics with a dimuon gun Monte Carlo and we propagate generator-level muon trajectories through the CMS magnetic field to the muon system, then plot efficiency as a function of the distance between the muons. Both of these techniques were used in Sec. 2, but here we plot the probability of reconstructing *both* muons offline, rather than the probability of triggering on one of the two. For barrel muons ($|\eta| < 1$), this surface is a cylinder centered on the beamline with radius 600 cm. For endcap muons ($|\eta| > 1$), this surface is a plane at 700 cm or -700 cm from the interaction point, perpendicular to the beamline (see Fig. 6). The distance of separation is quantified in the barrel as $\Delta\phi$ (difference in azimuthal angles) and $\Delta z/r$ (displacement parallel with the beamline divided by 600 cm), and in the endcap, the distance of separation is $\Delta\phi$ and $\Delta r/z$ (radial displacement toward or away from the beamline divided by 700 cm). Reconstruction probabilities are shown in Fig. 7 for the barrel and Fig. 8 for the endcap.

In all cases, the GlobalMuon efficiency follows the StandAloneMuon efficiency, and the reconstruction efficiency of two TrackerMuons is nearly independent of crossing distance. (The arbitration requirement introduces a 5% drop in efficiency for $|\Delta\phi| < 0.1$ muons in the endcap.) The barrel profile is complicated by the fact that propagated generator-level muons don't accurately predict the position of a real muon in the barrel,

people may not realize that you require one muon $p_T > 15$ GeV (may add a little reminder!)

Unclear!

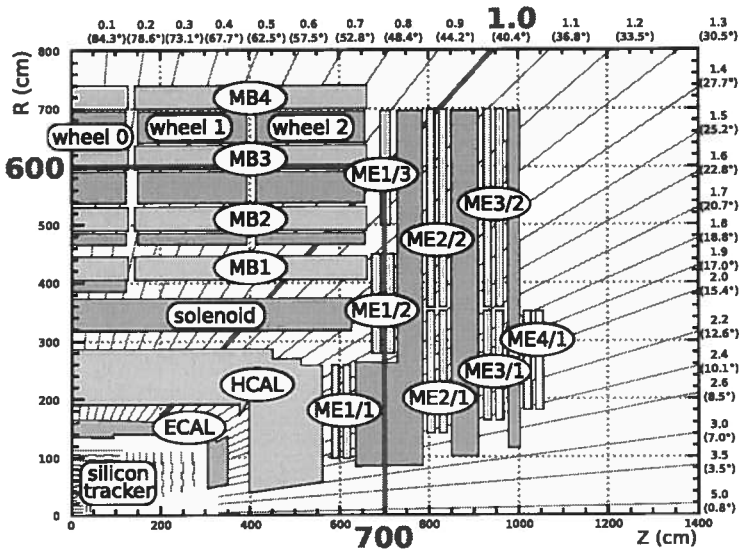

Figure 6: CMS quarter-view illustrating the cylindrical surface with 600 cm radius (barrel, $|\eta| < 1$) and plane 700 cm from the beamspot (endcap, $1 < |\eta| < 2.4$) used to quantify reconstruction efficiency as a function of crossing distance in the muon system.

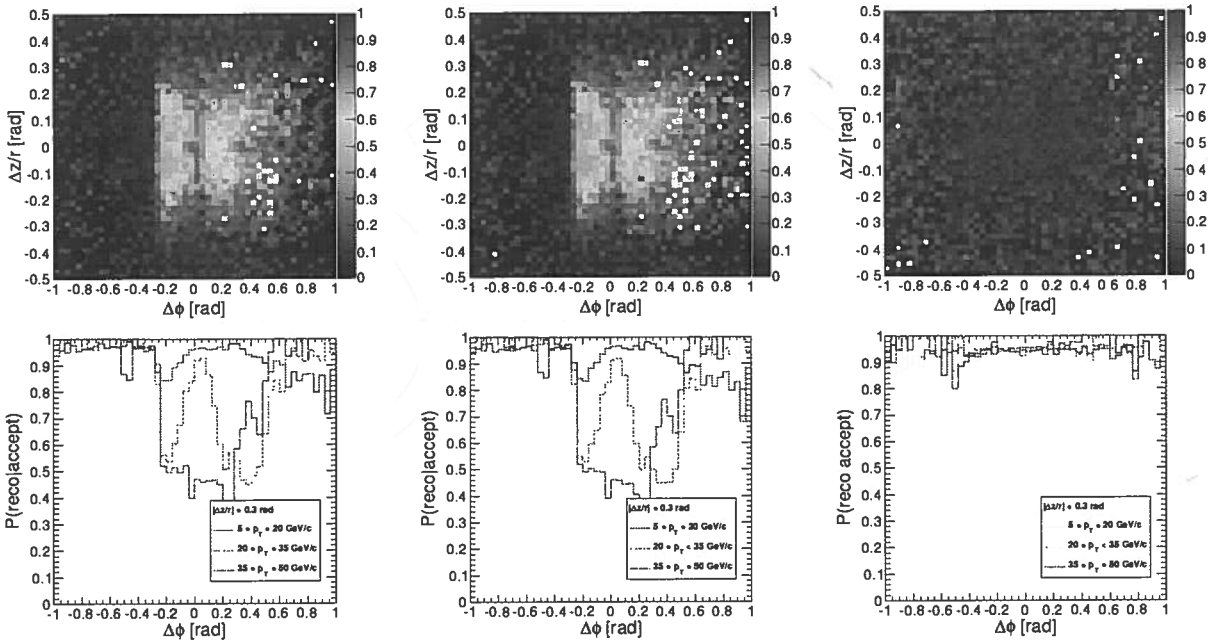

Figure 7: Probability of reconstructing two muons (both $|\eta| < 1$) as StandAloneMuons (left), GlobalMuons (middle), and TrackerMuons with quality cuts (right). Top row: efficiency versus distance between the muon trajectories on a cylinder of radius 600 cm. Bottom row: profile in $\Delta\phi$ ($|\Delta z/r| < 0.3$) with both muons in a given p_T range.

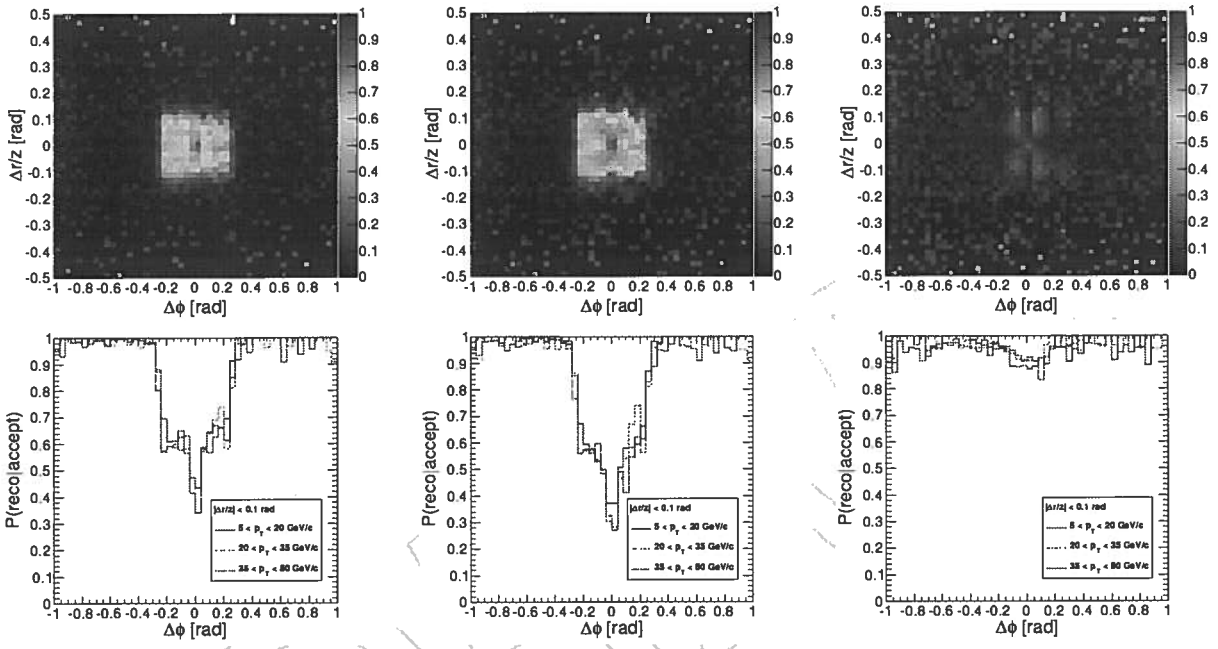

Figure 8: Probability of reconstructing two muons (both $|\eta| < 1$) as StandAloneMuons (left), GlobalMuons (middle), and TrackerMuons with quality cuts (right). Top row: efficiency versus distance between the muon trajectories on a plane ± 700 cm from the interaction point. Bottom row: profile in $\Delta\phi$ ($|\Delta r/z| < 0.1$) with both muons in a given p_T range.

since real muons can scatter or lose energy to a final-state photon. This is why the efficiency curve is smeared toward positive $\Delta\phi$ (energy loss in either muon would result in positive $\Delta\phi$) for low-momentum muons, forms two inefficient regions for mid-range momenta (two helix topologies, often called "cowboys" and "seagulls"), and a single inefficient region for $\Delta\phi = 0$.

To avoid these reconstruction inefficiencies, we use TrackerMuons for all offline muon identification. Section 4 describes how this efficiency is actually measured and applied per muon.

3.2 Offline muon fake rate

Raw TrackerMuons only require a tracker-track to be consistent with a segment in the muon system, but in dense tracking environments, several tracks from hadronic particles may point to the segments of a real muon and become incorrectly identified as additional muons. This would lead to an unacceptably high muon fake rate. GlobalMuons, on the other hand, are known to have low fake rates, but with the inefficiency for nearby muons described in Sec. 3.1.

TrackerMuons can be selected with the same purity as GlobalMuons by requiring at least two fully arbitrated segments. Full arbitration (SegmentAndTrackArbitration) requires only one segment to match to each tracker-track per chamber (SegmentArbitration) and only one tracker-track to match to each segment (TrackArbitration). The actual cut is placed on the number of matched segments with this property. This emulates an implicit condition in GlobalMuon reconstruction: segments used to build one muon are not available for any other muons.

Using a sample of realistic background Monte Carlo (inclusive muons with $\hat{p}_T > 30\ \mathrm{GeV}/c$) in Fig. 9, we show the distribution of the number of tracks for raw TrackerMuons, TrackerMuons with at least two segments and at least two arbitrated segments, and GlobalMuons as a reference. In Fig. 10, we show this plot for different numbers of matched generator-level muons. Both the number of reconstructed GlobalMuons and fully arbitrated TrackerMuons peak at the true number of muons with similar tails, demonstrating a similar fake rate.

The number of tracker hits and tracker-track χ^2 cuts have negligible impact on efficiency and fake rates, but they are standard track quality cuts.

4 Measuring trigger and offline muon efficiencies

FIXME: Need to get this number from somewhere. Surely it should be $J/\psi \to \mu\mu$ tag-and-probe, but with our cuts to be completely in the plateau efficiency region. It should be one event-level correction for the trigger efficiency and one efficiency factor per muon for the offline reconstruction.

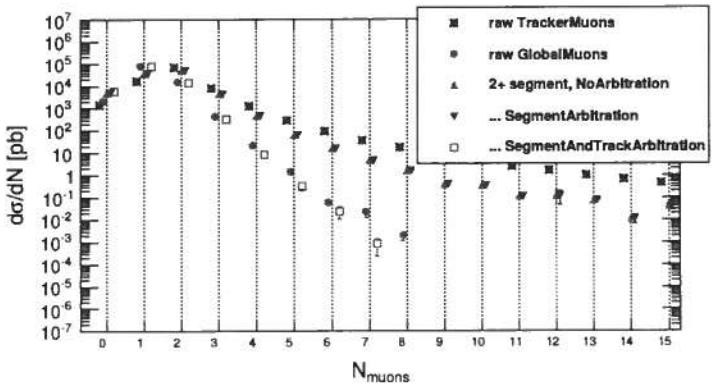

Figure 9: Number of reconstructed muons in an inclusive muon backgrounds sample with $\hat{p}_T > 30$ GeV/c. The fully arbitrated TrackerMuons has a purity similar to GlobalMuons.

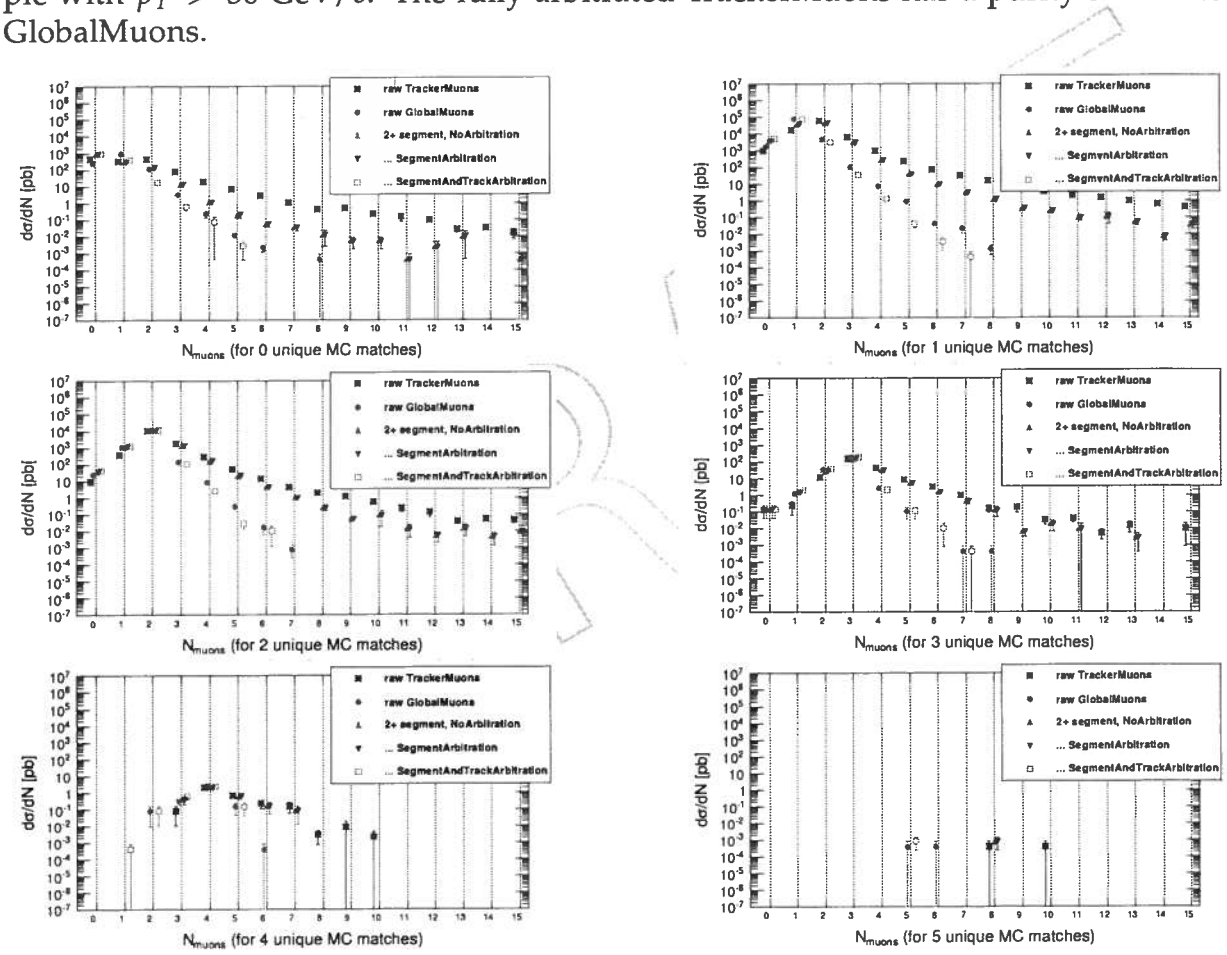

Figure 10: Number of reconstructed muons as in Fig. 9, split by the number of true muons in the event (unique MC matches). In each case, the fully arbitrated TrackerMuons and the GlobalMuons peak at the true number of muons with similar tails.

4.1 Mu-jet clustering and fundamental dimuon decomposition

Complicated lepton-jets cascades can make it difficult to identify which muons belong to which resonance, and therefore possibly misreconstruct the masses and fail to identify the signature. To be prepared for any high-multiplicity muon event with many boosted resonances, it is necessary to have a procedure to organize the muons into likely pairings and groups. Our organizational procedure has two steps: (1) groups of "close-by" muons are grouped into mu-jets with arbitrarily many mu-jets per group, and (2) mu-jets are analyzed for the most likely decomposition into fundamental dimuons belonging to the lowest-mass state in the hidden spectrum.

To cluster muons into mu-jets, we identify opposite-sign pairs of close-by muons according to pairwise invarant mass (m_{inv}) and pairwise vertex compatibility (P_{vertex}) and group all close-by muons. Muon tracks with very small angular separation ($\Delta R < 0.01$) have an increased probability of failing the vertex fit (Fig. 11), so we define two oppositely-charged muons as being close-by if the following is satisfied:

$$\left(m_{\text{inv}} < 5\ \text{GeV}/c^2 \textbf{ and } P_{\text{vertex}} > 0.01\right) \textbf{ or } \Delta R < 0.01. \tag{1}$$

This definition has the following consequences:

- any resonance with mass $< 5\ \text{GeV}/c^2$ decaying into two properly reconstructed muons is guaranteed to be considered close-by with 99% probability, regardless of momentum;
- muons originating from two different points in space are suppressed ($b \to \mu\mu X$ has about 75% efficiency);
- very small angle dimuons are not lost due to failure of the vertex fitter, but only these dimuons, with a relativistic boost of $\gamma > 100$, are exempt from the vertex test.

Close-by pairs are iteratively grouped into mu-jets until every pair of close-by muons are in the same mu-jet. Closeness is always defined between muons, never an averaged group of muons, so the clustering procedure is independent of the order in which it is applied. Whole decay chains in which the most massive state in the cascade has a mass under $5\ \text{GeV}/c^2$ would also be grouped into a single mu-jet, assuming that all final state muons are reconstructed.

To search for a mass peak corresponding to the lightest state in the hidden sector, mu-jets are decomposed into fundamental dimuons. In a mu-jet with many muons, there can be several ways to partition the muons into oppositely-signed pairs. One of these combinations minimizes the quantity

$$\chi^2_{\Delta m} = \sum_{i}^{\text{OS pairs}} \sum_{j>i}^{\text{OS pairs}} \left(m_i - m_j\right)^2. \tag{2}$$

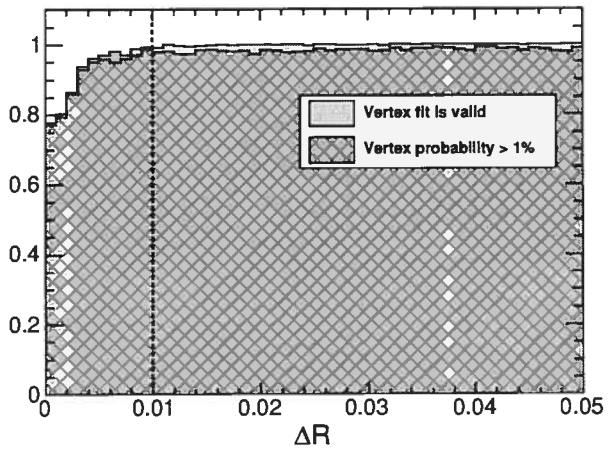

Figure 11: Probability of vertex fit failure and vertex compatibility > 1% as a function of geometric separation ($\Delta R = \sqrt{(\Delta\phi)^2 + (\Delta\eta)^2}$).

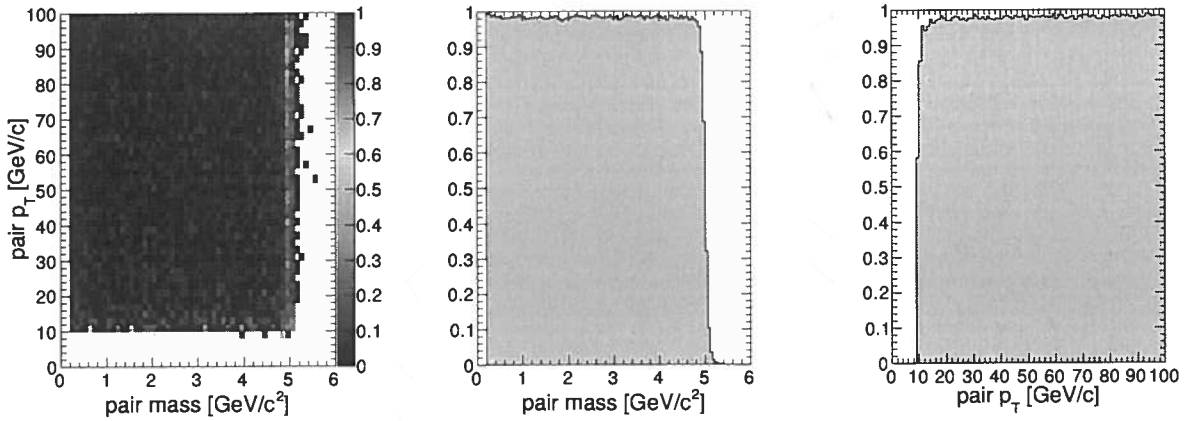

Figure 12: Probability to form a mu-jet, given two reconstructed muons.

This set of masses is most consistent with multiple instances of $m_1 \to \mu\mu$ overlapping one another in the same event.

Figures 12–15 demonstrate the uniformity of mu-jet efficiency over masses of $2m_\mu$–5 GeV/c^2 and momenta up to 100 GeV/c. Figure 12 shows the algorithmic efficiency, determined primarily by the $P_{\text{vertex}} > 1\%$ constraint. Figure 13 is the combined probability of track reconstruction and the clustering algorithm. The same for events with one $p_T > 15$ GeV/c, $|\eta| < 1$ muon (to satisfy the trigger) is shown in Fig. 14: it essentially raises the minimum mu-jet p_T from 10 GeV/c to 20 GeV/c. Finally, Fig. 15 shows the efficiency of the trigger, reconstruction, and mu-jet clustering.

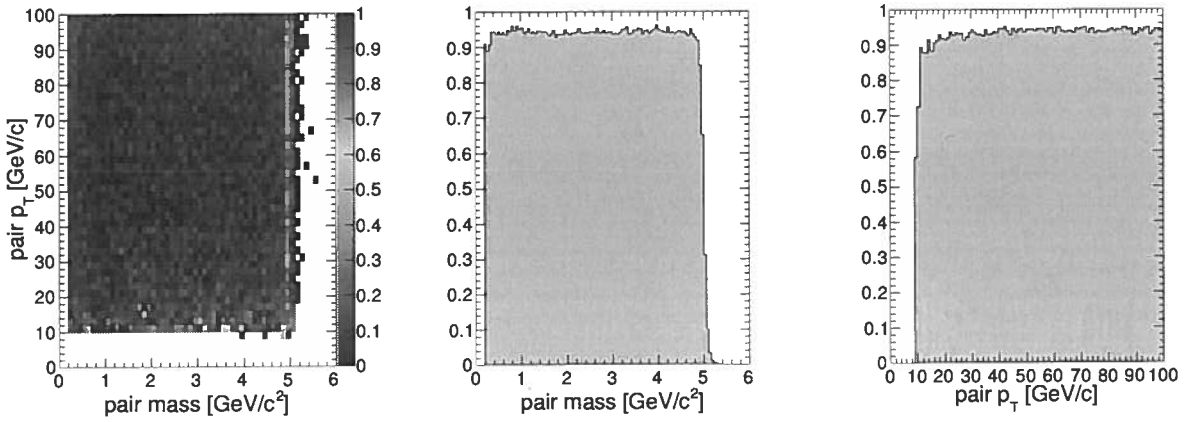

Figure 13: Probability to reconstruct two muons and form a mu-jet, given two muons with $p_T > 5$ GeV/c and $|\eta| < 2.4$.

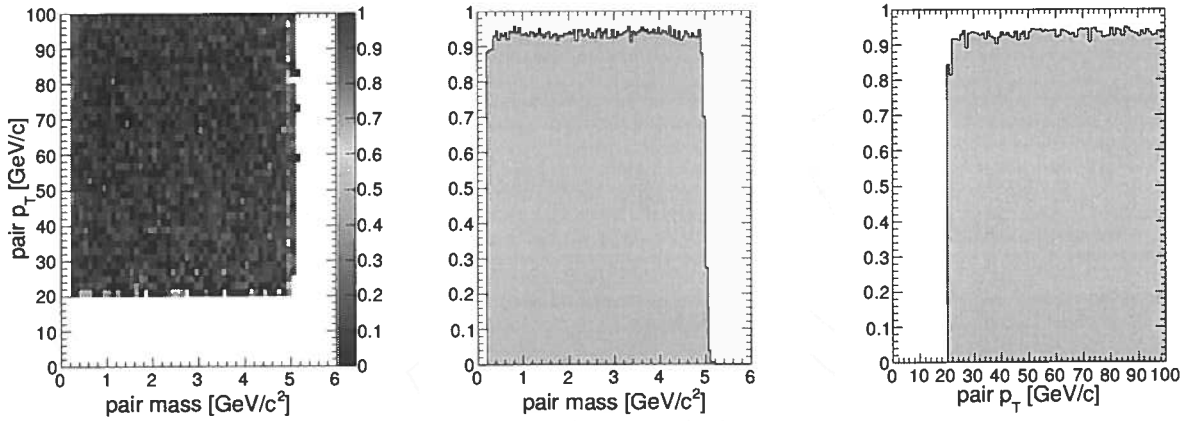

Figure 14: Probability to reconstruct two muons and form a mu-jet, given two muons, one with $p_T > 15$ GeV/c and $|\eta| < 1$, the other with $p_T > 5$ GeV/c and $|\eta| < 2.4$.

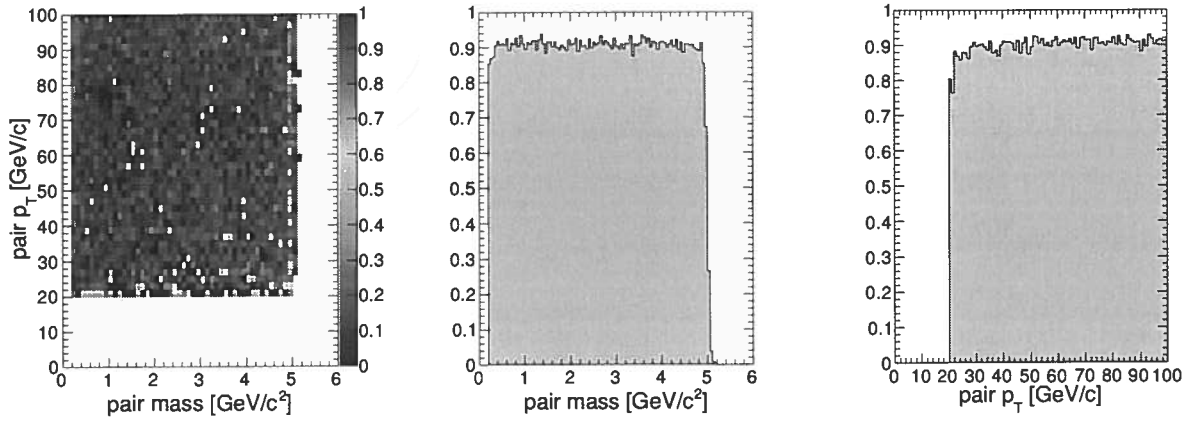

Figure 15: Probability to trigger, reconstruct, and form a mu-jet, given two muons, one with $p_T > 15$ GeV/c and $|\eta| < 1$, the other with $p_T > 5$ GeV/c and $|\eta| < 2.4$.

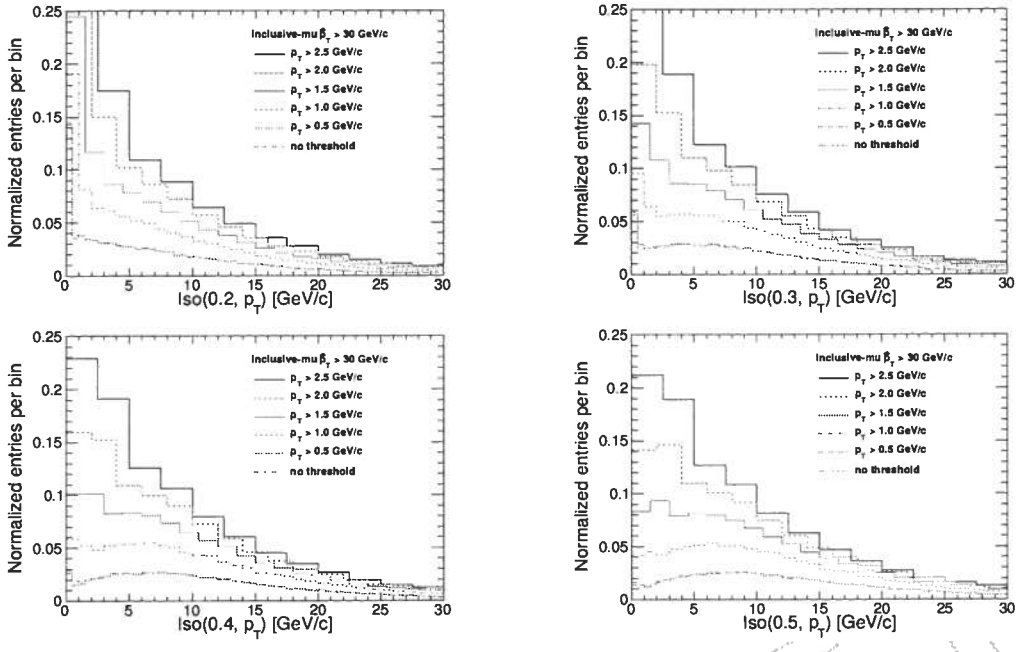

Figure 16: Inclusive muon MC ($\hat{p}_T > 30$ GeV/c) distributions of $Iso(R^{\max}, p_T^{\min})$. Histogram bins have the same width as the $p_T^{\min}$ threshold.

4.2 Mu-jet isolation

Although isolation is not applied to any signal regions, it is a useful tool for identifying background sources in the control samples and would be used to study a signal if one is discovered. Standard muon isolation is inappropriate because nearby muons would fall within each other's isolation cones. We therefore define a new track-based isolation variable that excludes all muons from the set of tracks. The isolation Iso of a mu-jet is

$$Iso(R^{\max}, p_T^{\min}) = \sum_{\text{non-}\mu \text{ tracks}} \begin{cases} p_T & \text{if } \Delta R < R^{\max} \text{ and } p_T > p_T^{\min} \\ 0 & \text{otherwise} \end{cases} \quad (3)$$

where ΔR is $\sqrt{(\Delta\phi)^2 + (\Delta\eta)^2}$ with respect to the mu-jet's momentum axis (vector sum of all grouped muon momenta). The cone radius $\Delta R < R^{\max}$ and track momentum threshold $p_T^{\min}$ are optimized such that Standard Model backgrounds from b-jets are roughly uniform in the range $0 < Iso \lesssim 10$ GeV/c.

Distributions of $Iso(R^{\max}, p_T^{\min})$ in Monte Carlo samples covering the range of backgrounds for our signal topologies are presented in Figs. 16 (inclusive muon with $\hat{p}_T > 30$ GeV/c), 17 (inclusive muon with $\hat{p}_T > 100$ GeV/c) and 18 ($b\bar{b} \to 4\mu\, X$ in two mu-jets). All have a roughly flat region in $0 < Iso < 10.5$ GeV/c for $\Delta R < R^{\max} = 0.4$ and $p_T^{\min} = 1.5$ GeV/c (lower-left plot, dotted blue curve in all Figures).

Figure 19 shows the same distributions for an idealized signal: a muon pair-gun with high pile-up (average of 5 interactions per crossing). From this we see that the isolation

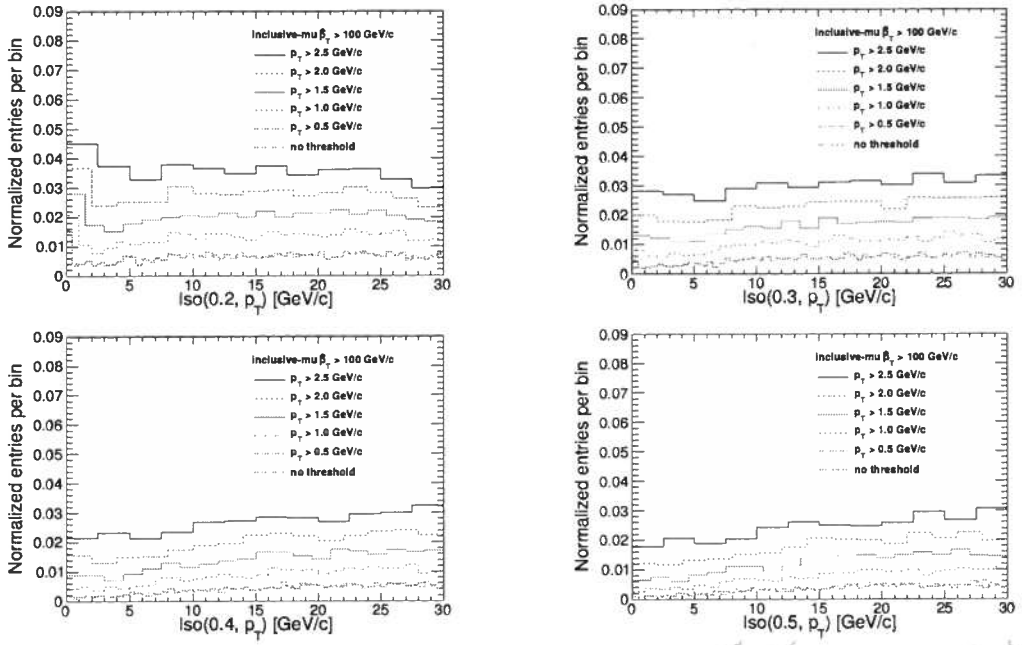

Figure 17: Inclusive muon MC ($\hat{p}_T > 100$ GeV/c) distributions of $Iso(R^{\max}, p_T^{\min})$. Histogram bins have the same width as the $p_T^{\min}$ threshold.

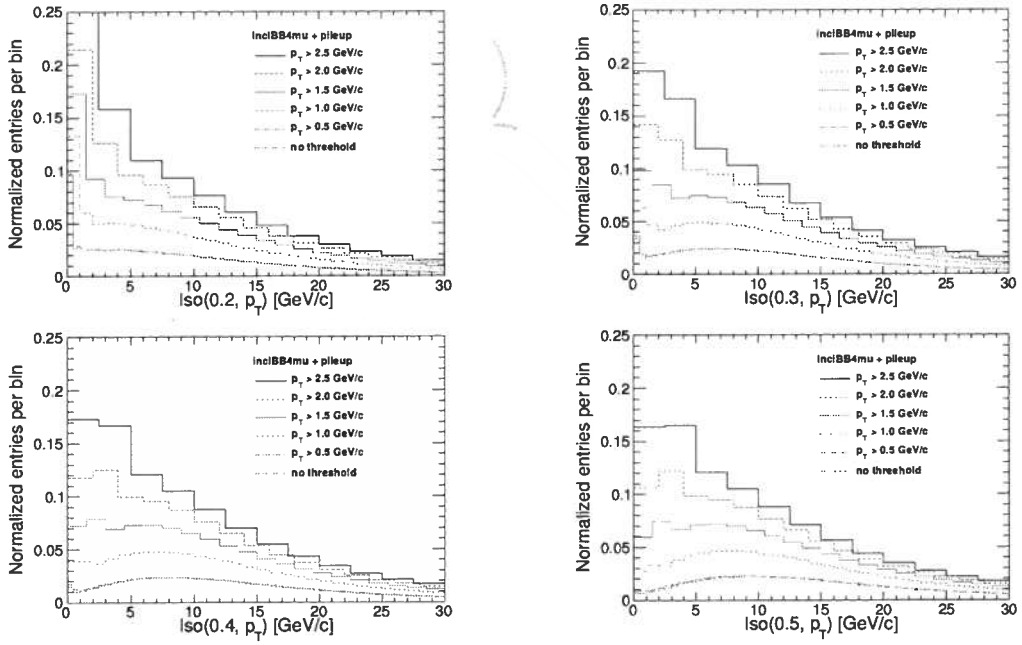

Figure 18: Muon-enriched $b\bar{b} \rightarrow 4\mu X$ MC ($\hat{p}_T > 30$ GeV/c) distributions of $Iso(R^{\max}, p_T^{\min})$. Histogram bins have the same width as the $p_T^{\min}$ threshold.

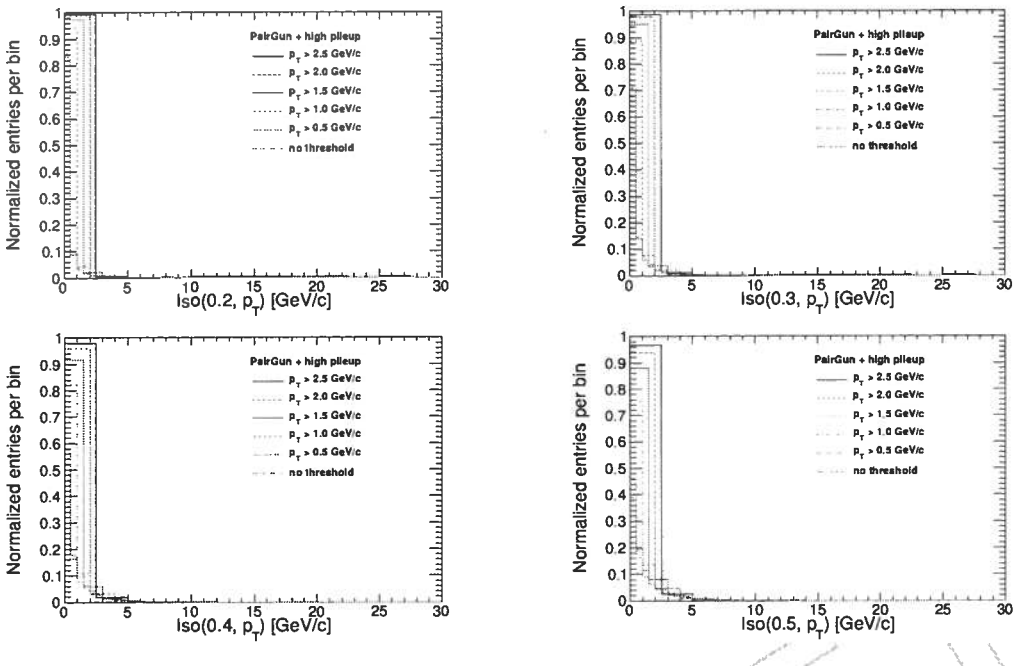

Figure 19: Muon pair-gun MC with high pile-up (average of 5 interactions per crossing) distributions of $Iso(R^{\max}, p_T^{\min})$. Histogram bins have the same width as the $p_T^{\min}$ threshold.

does not veto real muon pairs (most of which are within $\Delta R < 0.4$) and is insensitive to pile-up. In realistic lepton jets scenarios, mu-jets may be produced with e^+e^- or $\pi\pi$ and fail isolation for a fraction of the events (large for Z-like couplings, small for Higgs-like couplings).

The mu-jet clustering is defined with a cut on pairwise invariant mass, while isolation is defined with a geometric cone. It is therefore possible for two distinct mu-jets to have overlapping isolation cones. In such a case, the values of the isolation variables of the two mu-jets would be correlated by sharing tracks. However, the main source of backgrounds to two mu-jet events, $b\bar{b} \to 2\mu$, 2μ, are overwhelmingly back-to-back in ϕ. Figure 20 shows the separation of pairs of mu-jets from $b\bar{b}$: only very boosted $b\bar{b}$ systems produce mu-jets with overlapping isolation cones ($\Delta R \leq 2R^{\max} = 0.8$).

while not a concern for signal, it may introduce correlation in possible schemes relying on isolation to do background estimation.

5 Analysis of background control samples

FIXME: Some data/MC comparison plots, some free-form investigation of the data control sample, because I know that the background is not really all $b\bar{b}$. The $b\bar{b}$ part can provide templates for the two dimuon channel, but any Drell-Yan part can't. Isolation is one tool for distinguishing between $b\bar{b}$ and Drell-Yan, the vector-like vs. uncorrelated distribution of track angles in the dimuon's reference frame is another that I haven't looked at yet (it has been implemented). Need to reach some kind of conclusion about

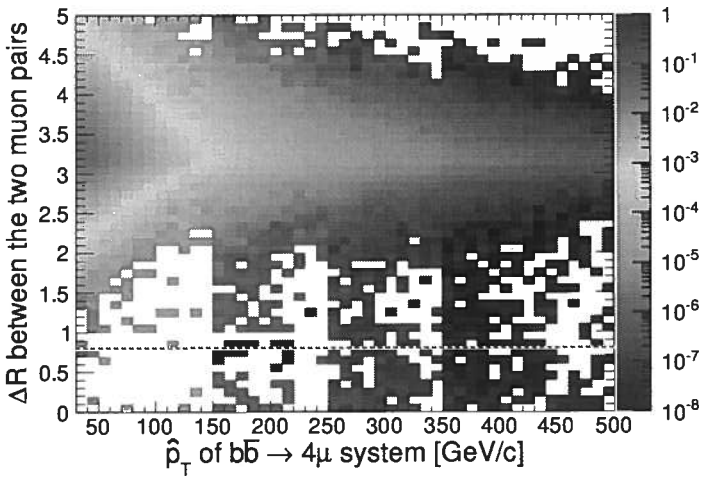

Figure 20: Separation of mu-jets in $b\bar{b} \to 2\mu$, 2μ backgrounds: most $b\bar{b}$ pairs are back-to-back in ϕ, making the geometric overlap of isolation cones ($\Delta R \leq 2R^{\max} = 0.8$) unlikely. This Monte Carlo sample was generated in bins of $\hat{p}_T$.

the low-mass excess: perhaps it's just a funny shape in the Drell-Yan (angular distributions would help with that). The Monte Carlo also shows you how the background is broken down into dimuons from real physics (almost 100%) and misreconstruction, decays-in-flight, unassociated muons that happened to be grouped (negligible).

6 Data-driven backgrounds estimates

FIXME: Getting template mass shapes from the control samples to apply to the signal regions. Single dimuon channel (a) comes from lower-momentum muons (but high enough for the non-isolated and isolated components to scale the same way—40 GeV/c). Single quadmuon channel (b) comes from 3 muons + track or 2 muons + 2 tracks (since you can only get quadmuons from misreconstruction of a random track as a muon). Single megamuon (c) comes from N extra tracks. Two dimuon (d-1) comes from squaring the single dimuon control sample, and is checked with the slice around J/ψ and isolation. One dimuon, one quadmuon (d-2) comes from multiplying the two mujet probability with the muons + tracks probabilities. It's small. Two quadmuons (d-3) is just products of muons + tracks. Very small. And anything more than that (e) is so small that maybe we don't need to set an estimate.

There could be signal here!!! (will affect the limit depending on p_T of the $\mu\mu$-jet)

7 Fitting and limit-setting

FIXME: A description of the technique. We have a working fitter that needs to be revived (it was used in a phenomenology study of the NMSSM case.) The fit only sets

the magnitude of the background— its shape is determined from control samples (or a fit to control samples for smoothing.)

8 Fit results in sample models

FIXME: The NMSSM is a good model, but tighter limits could be set with a more directed search. The Extra-U(1) is more like a straw man, but it provides examples of all the sorts of things that appear in realistic lepton jets models. There's a realistic lepton jets model produced by the Princeton group, and I'd like to test that if we could get access to it.

9 Fit results and limits on signatures

FIXME: We do the fit, get the result for the yield as a function of mass and background level below the mass peak (a fraction of an event), apply plateau trigger and muon-reconstruction efficiencies, and publish limits on $\sigma\mathcal{B}\alpha$ for the lowest-mass state in the hidden hierarchy (where α is the acceptance of the simple cuts described at the end of the Introduction). Also trial factors, which could be complicated.

9.1 (a) single dimuon

9.2 (b) single quadmuon

9.3 (c) single mu-jet with more than four muons

9.4 (d-1) two dimuons

9.5 (d-2) one dimuon, one quadmuon

9.6 (d-3) two quadmuons

9.7 (d-4) two mu-jets, one with more than four muons

9.8 (e) more than two mu-jets

10 Conclusions

A Sample event displays

B CMSSW software

`https://twiki.cern.ch/twiki/bin/view/CMS/ExoticaMuonJets`